ASEAN Engineering Journal

Full Paper

CLASSIFICATION OF HYDROGEN CONCENTRATIONS BASED ON TIO_2 GAS SENSOR RESPONSES USING ARTIFICIAL NEURAL NETWORK

Siti Amaniah Mohd Chachuli[a]*, A. Irfan Abdullah Pirus[a], M.N. Hamidon[b], Siti Asma Che Aziz[a], N.H. Shamsudin[c]

[a]Fakulti Teknologi dan Kejuruteraan Elektronik dan Komputer, Universiti Teknikal Malaysia Melaka, Hang Tuah Jaya, 76100 Durian Tunggal, Melaka, Malaysia
[b]Fakulti Kejuruteraan, Universiti Putra Malaysia, 43400 UPM Serdang, Selangor, Malaysia
[c]Fakulti Teknologi dan Kejuruteraan Elektrik, Universiti Teknikal Malaysia Melaka, Hang Tuah Jaya, 76100 Durian Tunggal, Melaka, Malaysia

Article history
Received
02 October 2024
Received in revised form
25 February 2025
Accepted
14 March 2025
Published online
30 November 2025

*Corresponding author
sitiamaniah@utem.edu.my

Graphical abstract

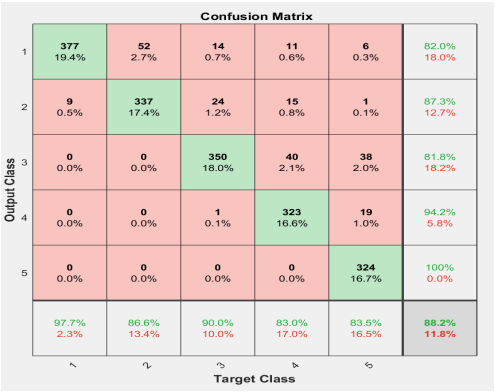

Abstract

In this research endeavor, a TiO_2 gas sensor was employed to discern the TiO_2 gas sensor response to varying hydrogen gas concentrations across three distinct temperature settings: 150℃, 200℃, and 250℃. The concentration levels spanned from 100 to 1000 ppm. The primary objective of this investigation was twofold: firstly, to eliminate the noise from the captured response, thereby clustering the gas sensor response at various hydrogen concentrations using principal component analysis, and secondly, to classify the hydrogen concentration using an artificial neural network. Five distinct hydrogen concentration values were extracted from each set of samples, in the range of 100 to 1000 ppm. All the values were acquired at different operational temperatures. The ensuing analytical phase utilizes the Principal Component Analysis (PCA) method in conjunction with an Artificial Neural Network (ANN). Remarkably, classification accuracy achieved a median testing accuracy of 88.8% in 70% of the training data and 15% of the testing strategy.

Keywords: TiO_2 gas sensor; principal component analysis; artificial neural network; gas classification

1.0 INTRODUCTION

Gas sensors are widely used in various fields, including environmental monitoring, industrial safety, and medical diagnosis. Because of its chemical stability and versatility in sensing different kinds of gases, the chemical-based gas sensor has drawn attention from researchers. Most chemical-based gas sensors using metal-oxide-semiconductor such as tin dioxide (SnO_2) [1]–[3], zinc oxide (ZnO) [4]–[6], tin dioxide (TiO_2) [7]–[9], tungsten oxide (WO_3) [10], [11], and indium oxide (In_2O_3) [12], [13]. Among the various gas-sensing materials, TiO_2 has attracted significant attention due to its superior sensitivity and stability, even in robust conditions [7]. TiO_2 gas sensors have been used to sense various types of gases such as hydrogen, nitrogen oxide, methane, carbon monoxide, etc. In our prior study, TiO_2 have been proven able to detect hydrogen [14], [15], thus transient response from our previous work will be classifiy in this study.

The concentration of hydrogen gas is a crucial factor in numerous industrial processes, including hydrogen fuel cells, chemical manufacturing, and petroleum refining. Moreover, hydrogen gas detection holds significant relevance in environmental contexts, particularly in monitoring air quality and ensuring workplace safety. Understanding how TiO_2 gas sensors respond to varying hydrogen concentrations is a fundamental aspect of optimizing their utility in real-world

applications. Temperature is paramount in gas sensing, as it can substantially affect the kinetics of gas-surface interactions, altering sensor responses. Hence, the investigation extends to different operating temperatures, providing a holistic assessment of sensor behavior.

Classification method have been widely used by many researchers to identify the type of data. This method has been applied in face recognition [16], [17], defects [18], [19], and etc. In gas sensing applications, principal component analysis (PCA) and neural networks have been applied to analyze sensor response data and classify the gas samples effectively. Machine learning methods for gas detection have been established including logistic regression, random forest, and support vector machines (SVM) [20]. Most of the classification techniques apply PCA and neural networks in gas sensing applications [2], [21], [22].

In classification of types of gas based on gas sensors, there are various methods have been reported in literature such as convolutional neural network (CNN) [2], [22], random forest [23], Recurrent Neural Network [24], and etc. Some researchers also proposed their algorithm such as eXtreme Gradient Boosting (XGB) [25], selective denoising autoencoder [26], and bidirectional recurrent neural network [27]. Most of these classification methods used numeric data as their input, such as current.

The ultimate objective is to categorize and classify sensor responses, utilizing advanced data analysis techniques, such as PCA and neural networks, to discern patterns and relationships between hydrogen concentrations at elevated operating temperatures. This work provides an organized process for data analysis and classification and develops the approach of classifying hydrogen concentrations at various operating temperatures of TiO_2 gas sensor based on their response value to the hydrogen.

2.0 METHODOLOGY

The process flow flowchart utilized in this investigation is displayed in Figure 1. A MATLAB software was used to classify the data from the TiO_2 gas sensor. The transient response of hydrogen response was obtained from our prior study [15]. The current measurement of was taken from one sample of TiO_2 gas sensor, which tested to hydrogen at different operating temperatures: 150℃, 200℃, and 250℃. Firstly, transient response data from the TiO_2 gas sensor was acquired as an initial step involving the generation of a MATLAB plot utilizing the provided parameter values. Subsequently, this MATLAB-generated plot is subjected to a comprehensive identification process. Once the successful plotting of the graph is achieved, the subsequent phase entails the representation of the noisy data, a necessary precursor for obtaining a smoothed transient response curve. Each of these curves undergoes a rigorous filtering procedure to enhance data clarity and reduce noise interference. After the successful execution of the filtering process, current values are meticulously extracted at distinct temporal intervals.

A three-dimensional cluster of data is constructed using the extracted current values within these predefined temporal ranges. This data cluster is then subjected to PCA, a statistical technique employed to reduce the dimensionality of the dataset. In this context, the objective is to reduce the multi-dimensional data into a two-dimensional representation. Subsequently, a comprehensive analytical assessment is undertaken to evaluate the efficacy of the clustering process and ascertain whether the data points within the resulting graph exhibit meaningful patterns or, conversely, lack discernible clustering. Finally to apply artificial neural network to the data to classify its concentration at different operating temperatures.

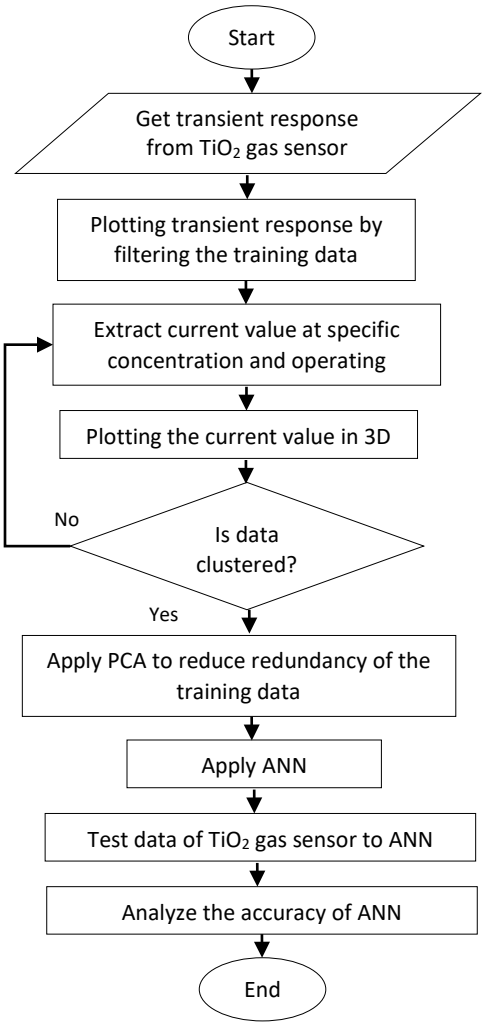

Figure 1 Flowchart of the process flow

3.0 RESULTS AND DISCUSSION

3.1 Transient Response And Filtered Response

Figure 2 shows the graphical representation elucidates the transient response characteristics and Figure 3 presents the filtered response of the TiO_2 gas sensor when exposed to a controlled concentration of hydrogen gas at an elevated temperature of 150℃, 200℃, and 250℃. It can be observed that the recorded response at 150℃ was captured with high noise. It also can be seen that the noise in the response can be dismissed when the operating temperature becomes higher; this is due to the current of the gas sensor becoming more

heightened and the sensor more conductive. Therefore, a filter has been used to remove the unwanted noise before the classification can be implemented. It can be observed that the noise in the gas sensor response has been eliminated. Next, the response at hydrogen concentration can be extracted at a certain time.

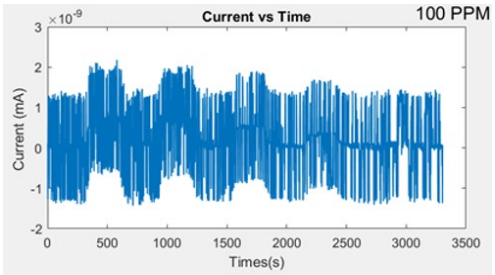

(a)

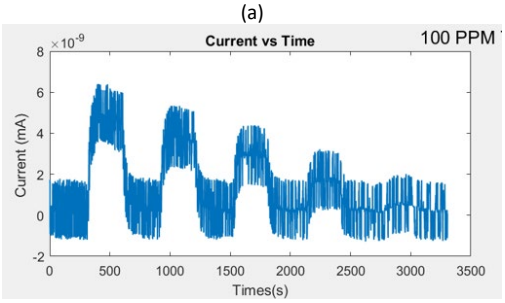

(b)

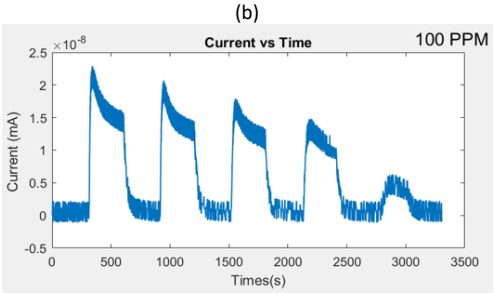

(c)

Figure 2 Before the filtering process of the transient response of TiO_2 gas sensor at different operating temperatures (a) (a) 150℃, (b) 200℃, and (c) 250℃

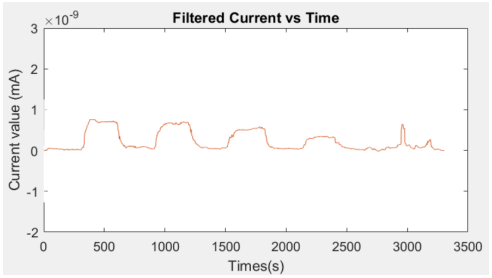

(a)

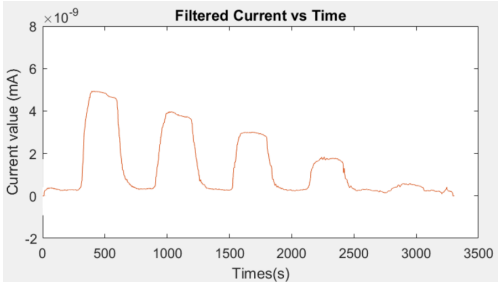

(b)

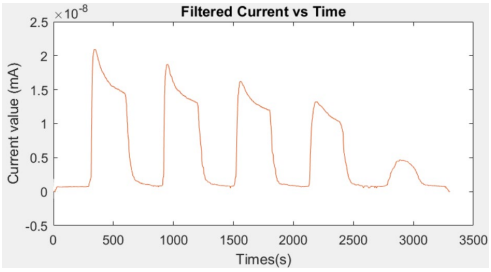

(c)

Figure 3 After filtering process of the transient response of TiO_2 gas sensor at different operating temperatures (a) 150℃, (b) 200℃, and (c) 250℃

3.2 Extraction Of Hydrogen Concentrations

From the filtered transient response, hydrogen concentrations of 100, 300, 500, 700, and 1000 ppm were identified. The transient response was recorded using the LabVIEW software. The software will capture the current value of the gas sensor and the mass flow controller (MFC) value of hydrogen and air during exposure to the gas sensor in sccm unit. Table 1 lists the hydrogen concentrations based on interval time at operating temperatures of 150℃, 200℃, and 250℃ with the setting sccm value used in the MFC. The sscm value of MFC for air was set to be the same during the whole measurement, and the hydrogen concentrations were varied by varying the MFC sccm value to obtain various hydrogen concentrations.

Table 1 Extraction of hydrogen concentration

Hydrogen concentration (ppm)	Sccm value for hydrogen	Sccm value for air	Interval time (s)
100	5	50	3000 – 3300
300	15	50	2100 – 2400
500	25	50	1500 – 1800
700	35	50	900 – 1200
1000	50	50	300 – 600

Figures 4, 5, and 6 display the extracted value for MFC (sccm value) for hydrogen and air, and the current value at operational temperatures: 150℃, 200℃, and 250℃. It can be seen that the sccm value for hydrogen and air were similar as listed in Table 1. The value of recorded current were too low, where the current is in the range of nA, thus the data was at the bottom of the graph (blue color), thus it cannot be seen in the graphs. Only the value of filtered currents were used for PCA and neural network analysis.

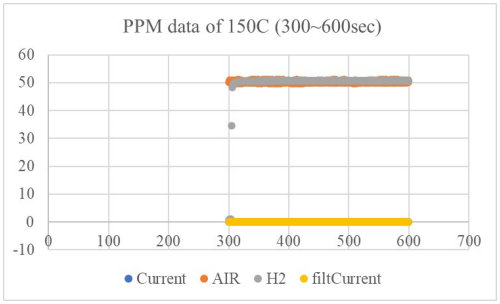

(a)

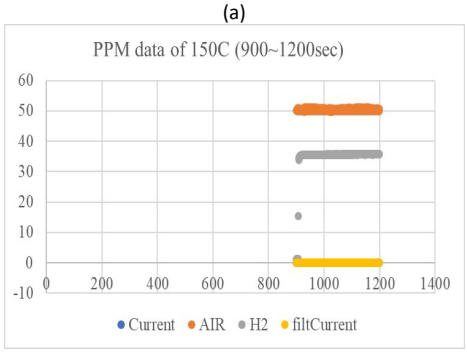

(b)

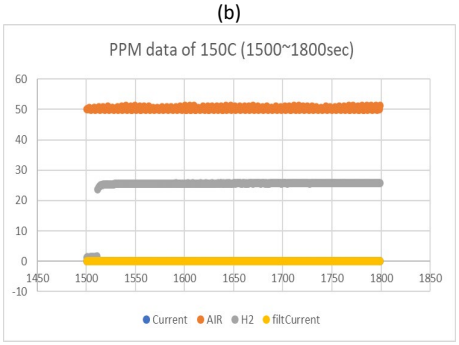

(c)

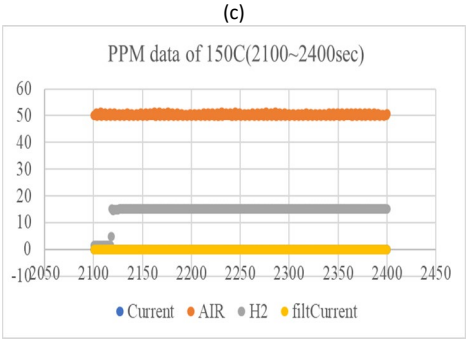

(d)

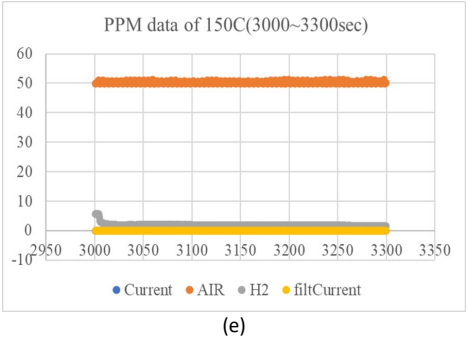

(e)

Figure 4 Extracted value of hydrogen concentrations at the operating temperature of 150°C (a) 1000 ppm, (b) 700 ppm, (c) 500 ppm, (d) 300 ppm, (e) 100 ppm

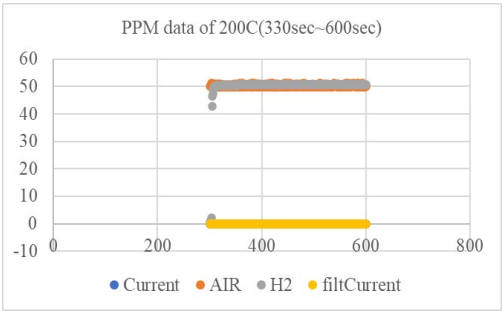

(a)

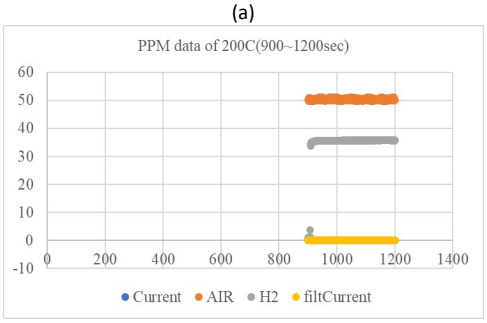

(b)

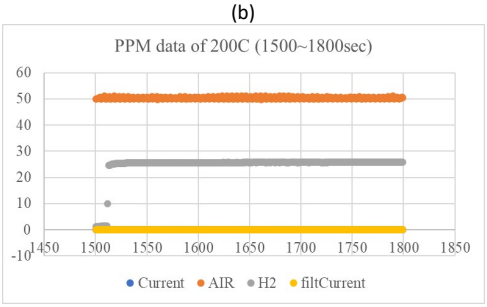

(c)

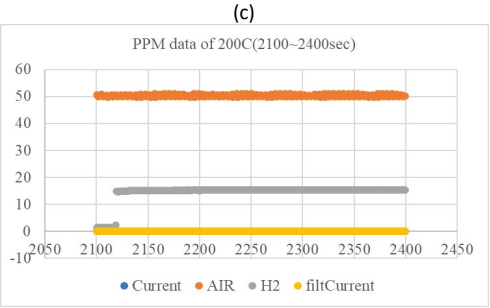

(d)

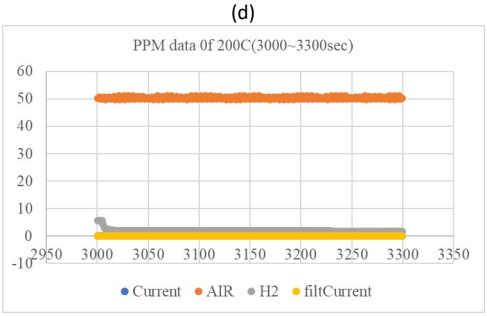

(e)

Figure 5 Extracted value of hydrogen concentrations at the operating temperature of 200°C (a) 1000 ppm, (b) 700 ppm, (c) 500 ppm, (d) 300 ppm, (e) 100 ppm

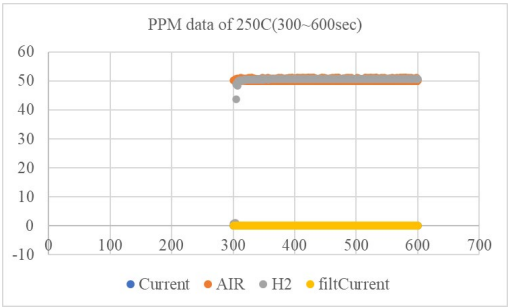

(a)

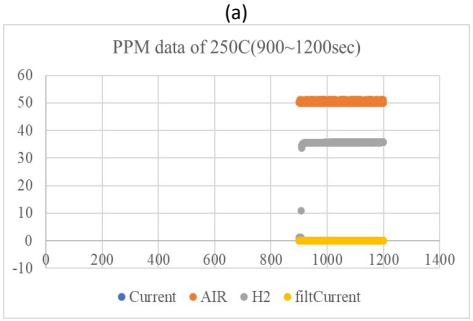

(b)

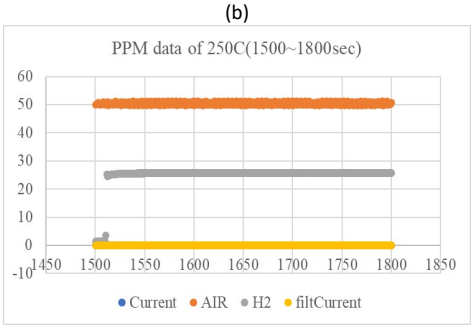

(c)

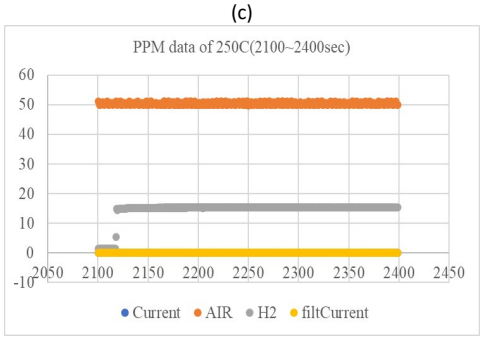

(d)

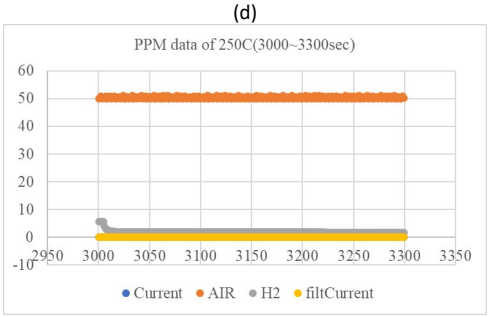

(e)

Figure 6 Extracted value of hydrogen concentrations at the operating temperature of 250°C (a) 1000 ppm, (b) 700 ppm, (c) 500 ppm, (d) 300 ppm, (e) 100 ppm

3.3 Analysis of Hydrogen Concentration Extraction Data using Principal Component Analysis

In broad terms, PCA can be understood as an orthogonal linear transformation wherein the eigenvalues represent the variances of data points when projected onto a line defined by their corresponding eigenvector direction. However, in the context of PCA implementation, a rotation around the multi-dimensional mean or central point is performed to align the base vectors with the principal components. Consequently, it is imperative that the data matrix is centered around the mean. For PCA analysis, the data was taken from the filtered current generated from Figures 4, 5, and 6. The results were plotted in 2-dimensional and 3-dimensional graphs to observe their relative parameters at different operating temperatures.

Figures 7, 8, and 9 illustrate PCA results in 2-dimensional and 3-dimensional with their Eigen values data that have been applied to 100 data points of hydrogen concentrations for operating temperatures of 150°C, 200°C, and 250°C, respectively. Red, green, blue, yellow, and pink color in Figures 6, 7, and 8 indicate data points for hydrogen concentration at 100 ppm, 300 ppm, 500 ppm, 700 ppm, and 1000 ppm, respectively. Reduced PCA shows the first eigenvalues of hydrogen concentration were large, the other two are small, as displayed in Figure 6(c), Figure 7(c), and Figure 8(c). It also can be observed that the data points were lying approximately on a line through the 3D mean with orientation parallel to the first eigenvectors. It can be seen that the weight was approximately 60%, 34%, and 7% at eigenvalues of 1, 2, and 3, respectively. Otherwise, the first eigenvalues were much larger than the second means that there is a direction that explains most of the data variance. This showed that a line exists that fits well with the data points. PCA plot converts the correlation among all of the cells into a 3-D graph. The established correlation is thus useful in achieving the distinct separation between the various hydrogen concentrations.

(a)

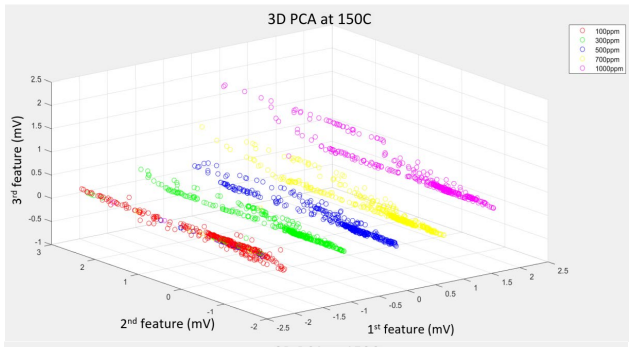

(b)

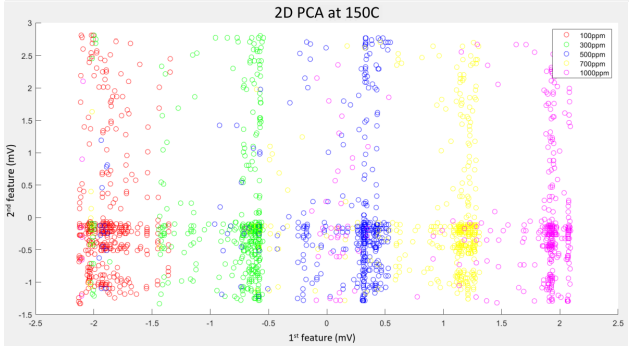

(c)

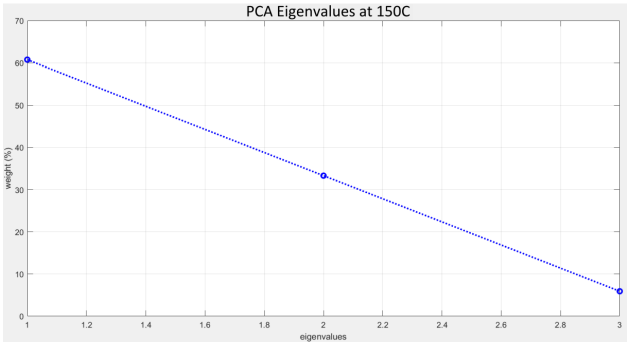

Figure 7 PCA results of TiO_2 gas sensor at operating temperature of 150℃ (a) 3D, (b) 2D and (c) Eigenvalue

(a)

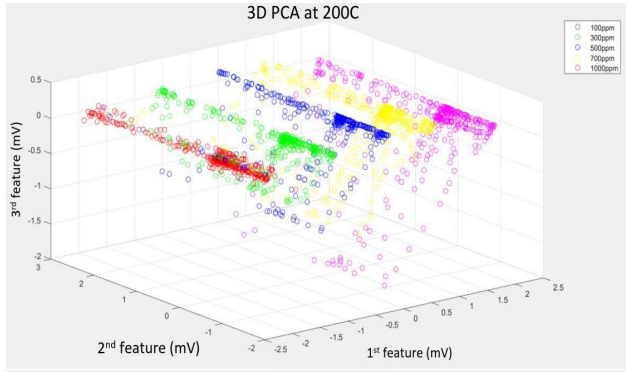

(b)

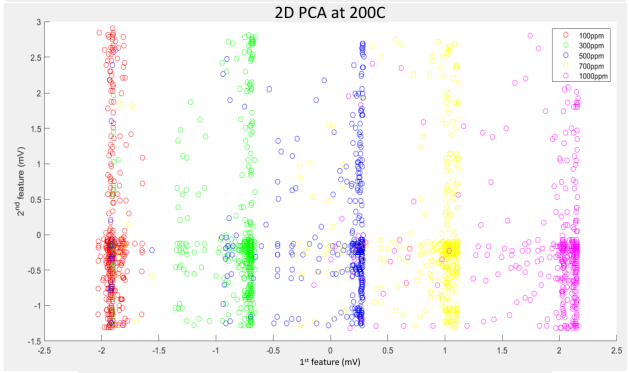

(c)

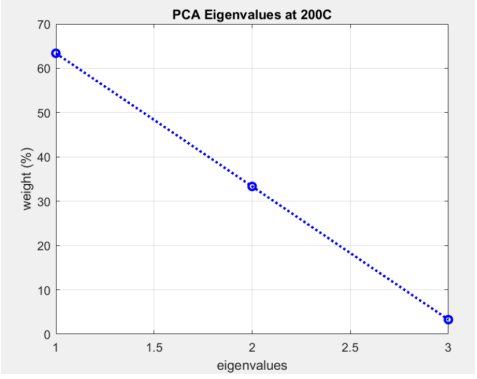

Figure 8 PCA results of TiO_2 gas sensor at operating temperature of 200℃ (a) 3D, (b) 2D and (c) Eigenvalue

(a)

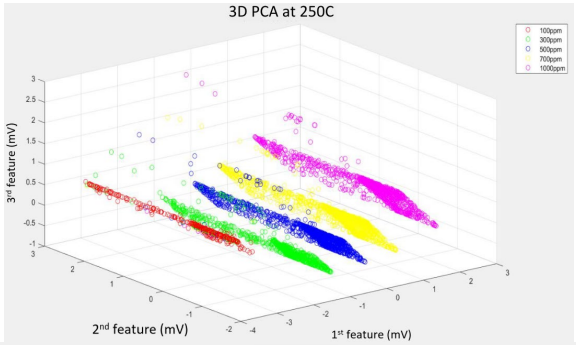

(b)

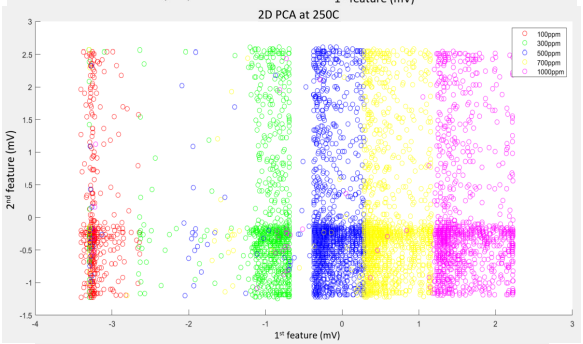

(c)

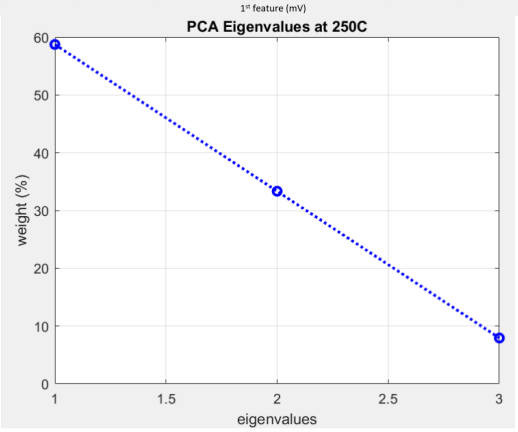

Figure 9 PCA results of TiO_2 gas sensor at operating temperature of 250℃ (a) 3D, (b) 2D and (c) Eigenvalue

3.4 Analysis on Artificial Neural Network

The pattern recognition of the forward neural network utilized in this investigation is shown in Figure 10. Ten neurons are present in the hidden layer. Approximately 70% of the original data was used to train the data. 1941 data points have been used to train the data, including all operating temperatures.

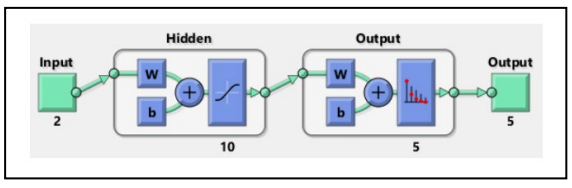

Figure 10 Pattern recognition for feed-forward the neural network

Figure 11 displays the neural network data's greatest validation performance. The training, validation, and testing data are displayed on the performance graph. The training data comprises 70%, whilst the validation and testing data consist of

approximately 15%. As epochs progress, the ANN's mean square error (MSE) has reduced. Given that its MSE at epoch 50, which is 0.075346, is nearly zero at the end of the training phase, indicating that it is a trained artificial neural network. When the MSE is small, or nearly zero, it indicates that the training set's ANN outputs and the intended outputs have gotten extremely near to one another. Figure 12 displays an error histogram of neural network data. The error histogram, using 20 bins, visualizes the discrepancies between target values and predicted values after training a feed-forward neural network.

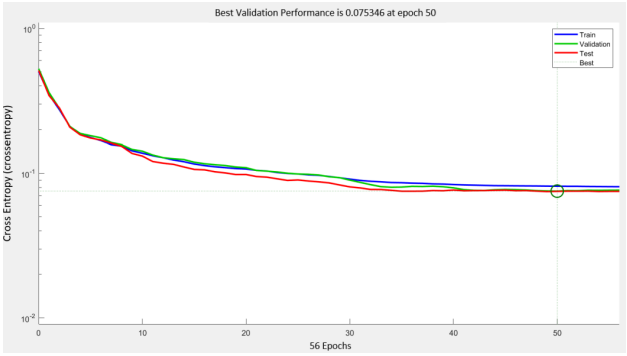

Figure 11 Best validation performance of neural network data

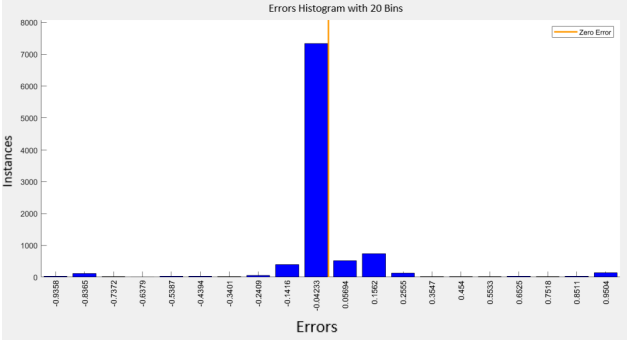

Figure 12 Error histogram of neural network data

The performance of a classification algorithm of TiO_2 gas sensor response to varied hydrogen concentrations at different operating temperatures is summarized in Figure 13, which displays the confusion matrix for 70% of the training data and 15% of the testing data method. It illustrates that the more data is used for the training phase, the more accuracy the model will achieve. The deep learning architecture for the TiO_2 gas sensor, which responds to varying hydrogen concentrations at elevated operating temperatures, has reached a median testing accuracy of 88.8% in the 70% training data and 15% of the testing strategy at the end of the training phase. These results indicated that more data in the architecture gives better accuracy where the architecture can be achieved.

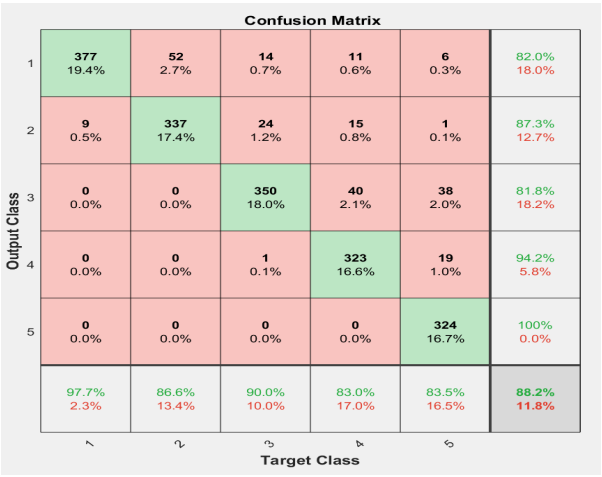

Figure 13 Matrix Confusion of TiO_2 gas sensor

4.0 CONCLUSION

The raw data of TiO_2 gas sensors with various concentrations of hydrogen at different operating temperatures have been successfully analyzed. There are several steps that need to be implemented before classification can be applied, including noise filtration and extraction of hydrogen response at a certain time. The classification can be started by using principal component analysis. With 70% of the training data and 15% of the testing strategy, the deep learning architecture for the TiO_2 gas sensor—which responds to varying hydrogen concentrations at elevated operating temperatures—has achieved a median testing accuracy of 88.8%.

Acknowledgement

The authors wish to extend their gratitude to Universiti Teknikal Malaysia Melaka (UTeM) for their support in providing funding to successfully complete the research under research grant no: PJP/2024/FTKEK/PERINTIS/SA0016.

Conflicts of Interest

The author(s) declare(s) that there is no conflict of interest regarding the publication of this paper.

References

[1] D. An, J. Dai, Z. Zhang, Y. Wang, N. Liu, and Y. Zou, 2024. "rGO/SnO_2 nanocomposite based sensor for ethanol detection under low temperature," *Ceramics International*, 50(9): 16272–16283, DOI: 10.1016/j.ceramint.2024.02.107.

[2] J. Y. Kim, S. P. Bharath, A. Mirzaei, S. S. Kim, and H. W. Kim, 2023, "Identification of gas mixtures using gold-decorated metal oxide based sensor arrays and neural networks," *Sensors Actuators B: Chemical,* 386: 133767, DOI: 10.1016/j.snb.2023.133767.

[3] J. Li et al., 2023, "Low-temperature and high-sensitivity Au-decorated thin walled SnO_2 nanotubes sensor for ethanol detection," *Materials Today Communications,* 37: 107217, doi: 10.1016/j.mtcomm.2023.107217.

[4] V. S. Chandak, M. B. Kumbhar, and P. M. Kulal, 2024. "Highly sensitive and selective acetone gas sensor-based La-doped ZnO nanostructured thin film," *Materials Letters,* 357: 135747, DOI: 10.1016/j.matlet.2023.135747.

[5] X. Sun et al., 2024, "UV-activated AuAg/ZnO microspheres for highperformance methane sensor at room temperature," Ceramics International, 50(17PB): 30552–30559, DOI: 10.1016/j.ceramint.2024.05.352.

[6] [6] J. Chao, D. Meng, K. Zhang, J. Wang, L. Guo, and X. Yang, 2024. "Development of an innovative ethanol sensing sensor platform based on the construction of Au modified 3D porous ZnO hollow microspheres," *Materials Research Bulletin,* 170: 112569, DOI: 10.1016/j.materresbull.2023.112569.

[7] L. B. Tasyurek, E. Isik, I. Isik, and N. Kilinc, 2024, "Enhancing the performance of TiO_2 nanotube-based hydrogen sensors through crystal structure and metal electrode," *International Journal of Hydrogen Energy.* 54: 678–690, DOI: 10.1016/j.ijhydene.2023.08.202.

[8] I. Nainggolan, W. T. Wadana, T. I. Nasution, and A. Sembiring, 2024, "The sensitivity of chitosan/TiO_2 film on ammonia detection," *Materials Today: Proceedings*, 0–7, DOI: 10.1016/j.matpr.2024.03.013.

[9] S. Amaniah Mohd Chachuli, M. Nizar Hamidon, M. Ertugrul, M. S. Mamat, H. Jaafar, and N. H. Shamsudin, 2020, "TiO_2/B_2O_3 thick film gas sensor for monitoring carbon monoxide at different operating temperatures," *Journal of Physics: Conference Series*. 1432(1), DOI: 10.1088/1742-6596/1432/1/012040.

[10] Y. Wang et al., 2023, "CuO/WO_3 hollow microsphere P-N heterojunction sensor for continuous cycle detection of H_2S gas," *Sensors Actuators B: Chemical*, 374: 132823, DOI: 10.1016/j.snb.2022.132823.

[11] L. Piliai et al. 2023. "NAP-XPS study of surface chemistry of CO and ethanol sensing with WO_3 nanowires-based gas sensor," *Sensors Actuators B: Chemical,* 397 DOI: 10.1016/j.snb.2023.134682.

[12] D. L. Kong et al., 2023 "Ag-nanoparticles-anchored mesoporous In_2O_3 nanowires for ultrahigh sensitive formaldehyde gas sensors," *Materials Science and Engineering: B,* 291. DOI: 10.1016/j.mseb.2023.116394.

[13] M. B. Kgomo, K. Shingange, M. I. Nemufulwi, H. C. Swart, and G. H. Mhlongo, 2023. "Belt-like In_2O_3 based sensor for methane detection: Influence of morphological, surface defects and textural behavior," *Materials Research Bulletin*, 158: 112076, DOI: 10.1016/j.materresbull.2022.112076.

[14] S. Amaniah, M. Chachuli, M. Nizar, H. Mehmet, E. Shuhazlly, and M. Omer, "Comparative analysis of hydrogen sensing based on treated - TiO_2 in thick film gas sensor," *Applied Physics A: Materials Science and Processing,* 128(7). DOI: 10.1007/s00339-022-05738-z.

[15] S. A. Mohd Chachuli et al. 2024, "Effects of silver diffusement on TiO_2-B_2O_3 nanocomposite sensor towards hydrogen sensing," *Materials Research Innovations.* 1–14 DOI: 10.1080/14328917.2024.2304480.

[16] K. Siwek and S. Osowski, 2018, "Deep neural networks and classical approach to face recognition – Comparative analysis," *Przegląd Elektrotechniczny*, 94(4): 3–6. DOI: 10.15199/48.2018.04.01.

[17] X. Yang, Z. Wang, H. Wu, L. Jiao, Y. Xu, and H. Chen, 2023, "Stable and compact face recognition via unlabeled data driven sparse representation-based classification," Signal Processing: Image Communication, 11: 116889, DOI: 10.1016/j.image.2022.116889.

[18] P. Kluge, 2021, "Methods for the classification and selection of extracted features of insulation defects from PD," *Przegląd Elektrotechniczny,* 1(6): 79–82, DOI: 10.15199/48.2021.06.14.

[19] T. Zhou, X. Zhu, H. Yang, X. Yan, X. Jin, and Q. Wan, 2023, "Identification of XLPE cable insulation defects based on deep learning," *Global Energy Interconnection,* 6(1): 36–49, DOI: 10.1016/j.gloei.2023.02.004.

[20] P. Narkhede, R. Walambe, S. Mandaokar, P. Chandel, K. Kotecha, and G. Ghinea, 2021. "Gas detection and identification using multimodal artificial intelligence based sensor fusion," *Applied System Innovation,* 4(1): 1–14. DOI: 10.3390/asi4010003.

[21] J. Oh et al. 2022., "Machine learning-based discrimination of indoor pollutants using an oxide gas sensor array: High endurance against ambient humidity and temperature," *Sensors Actuators B: Chemical,* 364: 131894, DOI: 10.1016/j.snb.2022.131894.

[22] J. Chu et al., 2021, "Identification of gas mixtures via sensor array combining with neural networks," *Sensors Actuators B: Chemical*. 329: 129090, DOI: 10.1016/j.snb.2020.129090.

[23] X. Chen, Q. Xing, X. Tang, Y. Cai, and M. Zhang, 2024, "Machine learning algorithm assisted cerium oxide based high selectivity acetone sensor," *Ceramics International,* 50(21PA): 41770–41779, DOI: 10.1016/j.ceramint.2024.08.030.

[24] N. Lim et al., 2024. "Enhancing mixed gas discrimination in e-nose system: Sparse recurrent neural networks using transient current fluctuation of SMO array sensor," *Journal of Industrial Information Integration*, 42: 100715, DOI: 10.1016/j.jii.2024.100715.

[25] B. Wang et al., 2023. "Artificial olfaction based on tafel curve for quantitative detection of acetone ethanol gas mixture," *Sensors Actuators B: Chemical,* 377: 2–9, doi: 10.1016/j.snb.2022.133049.

[26] I. Sohn et al., 2025, "Selective denoising autoencoder for classification of noisy gas mixtures using 2D transition metal dichalcogenides," *Talanta*. 283: 127129, DOI: 10.1016/j.talanta.2024.127129.

[27] Z. Wang et al., 2024. "Improved deep bidirectional recurrent neural network for learning the cross-sensitivity rules of gas sensor array," *Sensors Actuators B: Chemical,* 401: 134996, DOI: 10.1016/j.snb.2023.134996.